Discrete element modeling of hot mix asphalt complex modulus using realistic aggregate shapes

Juan Carlos Quezada Guajardo, Cyrille Chazallon

RESEARCH ARTICLE

Discrete element modeling of hot mix asphalt complex modulus using realistic aggregate shapes

Juan Carlos Quezada[a]* and Cyrille Chazallon[a]

[a]ICUBE, UMR 7357, CNRS, INSA de Strasbourg, Strasbourg, France

ARTICLE HISTORY
Compiled February 9, 2022

ABSTRACT
Asphalt mixtures are complex multiphase materials showing a viscoelastic behavior. In order to assess the mechanical response under traffic of these materials, a typical practice is to perform a complex modulus test. An alternative to laboratory characterization is to simulate numerically the complex modulus test by means of a discrete approach. Classical discrete approaches are able to reproduce the mechanical performances of asphalt mixtures, but show some difficulties to model non-spherical particles. In this work, the complex modulus test is reproduced numerically for an asphalt mixture by 3D simulations carried out with the LMGC90 code. A viscoelastic contact law is used to handle the interaction between particles with irregular shapes. The numerical aggregates were generated using the particle size distribution (PSD), the flakiness index (FI), and statistic data of actual aggregates, without using complex imaging techniques. Experimental and numerical testing campaigns were conducted for the complex modulus test on trapezoidal samples in a two-point bending (2PB) configuration. The numerical model was able to reproduce the mechanical performances obtained during the experimental tests, regarding the viscoelastic properties of the material. The influence on the mechanical performances of particle shape considering irregular aggregate was analyzed. The proposed model can be used to simulate the mechanical response of road surface layers under traffic loading.

KEYWORDS
Discrete element approach, Contact Dynamics method, 2PB complex modulus test, irregular particles, Burgers contact model.

1. Introduction

Hot mix asphalt is a complex multiphase system consisting of aggregates, mastic of bitumen and air. In this mixture the solid phase, composed of crushed aggregates, is binded with bitumen to ensure cohesion to the material. The aggregates can be identified as a granular material, where solid particles interact between them. On the other hand, the mastic phase shows a thermo-sensitive viscoelastic behavior. Thus, the mechanical performances of the mixture are dependent on temperature and strain rate. This macroscopic behavior is highly related to micro-scale behavior. Therefore, to predict the behavior of the pavement on a macroscopic scale, it is necessary to understand the micromechanical behavior of bituminous mixes.

*Corresponding author. Tel.: +33 3 88 14 47 84. Email: juan-carlos.quezada@insa-strasbourg.fr

To quantify the viscoelastic properties of these mixtures, such as the norm of the complex modulus $|E^*|$ and the associate phase angle Φ, it is usual to carry out a complex modulus test. These parameters are employed to compute the mechanical response of asphalt concrete under traffic (Chabot, Chupin, Deloffre, & Duhamel, 2010). Laboratory tests measure the macro-scale behavior of asphalt mixes at large-scale, but this approach cannot identify the behavior at the particle-scale. Numerical methods such as the Finite Element Method (FEM) use continuum mechanics approach to describe the macro-scale behavior of viscoelastic materials (Ameri, Mansourian, Khavas, Aliha, & Ayatollahi, 2011; Bai, Cheng, Hu, Fuentes, & Walubita, 2020; Chazallon, Koval, Hornych, Allou, & Mouhoubi, 2009; A. Collop, Scarpas, Kasbergen, & de Bondt, 2003; Dai & You, 2007; Fedele, Praticò, & Pellicano, 2019; He, Abdelaziz, Chen, & Yin, 2019; Kim, Allen, & Little, 2007; Li, Wang, Xu, & Xie, 2017; Y. Lu & Wright, 1998; Masad & Somadevan, 2002). However, these numerical methods struggle as experimental approaches to provide mechanical information at the particle-scale.

One way to solve this problem is by performing numerical simulations by means a discrete approach. This numerical method models the interaction of independent rigid or deformable bodies in contact. In the last years, the Discrete Element Method (DEM) has been broadly employed to simulate the mechanical performances of asphalt mixes (Abbas, Masad, Papagiannakis, & Harman, 2007; Buttlar & You, 2001; Dondi et al., 2014; Gao, Koval, & Chazallon, 2019; McDowell, Collop, & Wu, 2009; Nguyen, Froiio, Cambou, Di Benedetto, & Sauzéat, 2016; Quezada, Sagnol, & Chazallon, 2017; Yu & Shen, 2013; Zhou, Zhang, Li, Lu, & Chen, 2019).

In these studies, the mortar is simulated by a viscoelastic law interacting with particles at contact. Nevertheless, most of the studies have modeled the aggregates using spherical particles, simplifying the overall shape. In a granular material, the particle shape plays a major role regarding fabric anisotropy, force transmission and friction mobilization (Alonso-Marroquin & Herrmann, 2002; Azéma, Radjai, & Dubois, 2013; Azéma, Radjai, & Saussine, 2009; Cantor, Azéma, Sornay, & Radjai, 2017; Kim & Aragão, 2013; M. Lu & McDowell, 2007; Quezada, Breul, Saussine, & Radjai, 2012; Saint-Cyr et al., 2012; Souza, Kim, Souza, & Castro, 2012).

For the simulation of complex modulus properties, in most of numerical studies, the mechanical properties of the contact laws were empirically adjusted to match the macro-scale results from experimental data. This procedure results in using a generalized set of values in the contact law for every contact within a sample, where the variations of mechanical properties at the particle-scale are neglected. In some cases, this approach shows some divergences between numerical and experimental results.

In this work, laboratory 2PB complex modulus tests were conducted on trapezoidal samples to identify the viscoelastic properties of an asphalt mixture. Then, numerical 2PB tests were performed using a discrete approach with irregular particles. Finally, the results from numerical complex modulus tests were compared with the experimental data to validate the numerical approach.

In the following, Section 2 introduces the experimental procedures concerning the complex modulus tests performed in a 2PB configuration, the properties of the employed asphalt mixtures, the preparation protocol of experimental samples, the loading conditions and the calculation of the viscoelastic properties. Then, Section 3 presents the numerical procedures including the numerical method, preparation protocol, the characteristic of the adopted contact model and the 2PB test modeling. Finally, Section 4 measures the accuracy of the numerical results displaying the isotherms curves, master curves and analyzing the asymptotic behaviors for numerical and experimental data.

Table 1. Particle size distribution for the BBSG 0/10 Bréfauchet asphalt

Sieve size (mm)	12.5	10	8	6.3	4	2	1	0.5	0.25	0.125	0.063
PSD (%)	100	90	75	58	44	31	20	15	12	9	6.5

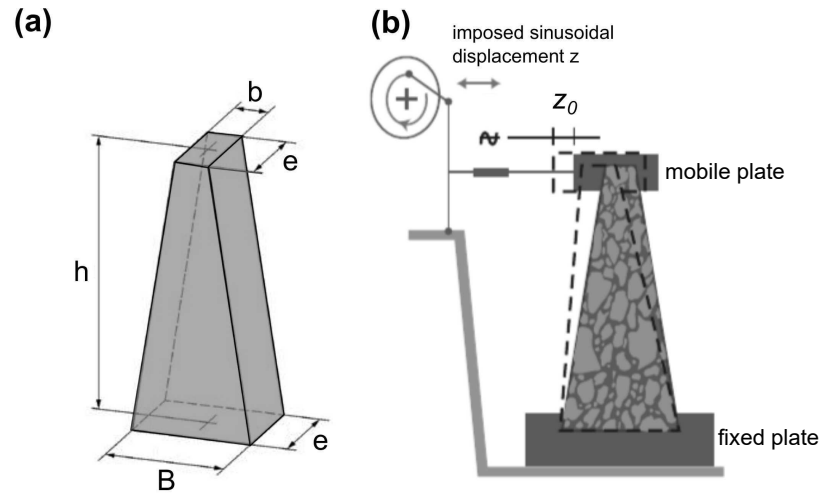

Figure 1. (a) Geometry and dimensions of the sample ("EN 12697-26: Bituminous mixtures. Test methods for hot mix asphalt. Part 26: Stiffness.", 2012). (b) Schema of the complex modulus test device.

2. Experimental procedures

2.1. Complex modulus test

The experimental campaign was conducted on trapezoidal samples, using a two point bending (2PB) configuration according to the EN 12697-26:2012 specification ("EN 12697-26: Bituminous mixtures. Test methods for hot mix asphalt. Part 26: Stiffness.", 2012).

For this campaign, four samples were manufactured using a Semi Coarse Asphalt Concrete (BBSG) 0/10 with a bitumen 35/50 grade, saw-cut from slabs manufactured in laboratory. Table 1 displays the particle size distribution (PSD) of the employed aggregates. Each trapezoidal specimen is 250 mm height, 56 mm at the bottom, 25 mm at the top and 25 mm width (Fig. 1a), with a total mass M about 0.6 kg, a bulk density of 2289 kg.m^{-3} and a void content of 4.7%.

For these experimental trials the frequency values tested were set at 3, 6, 10, 25 and 40 Hz, while the selected temperature values were -10, 0, 10, 15, 20 and 30 ^{o}C. On each sample, a sinusoidal displacement z is applied at the target frequency, with a peak displacement z_0 of 63×10^{-6} m, corresponding to a strain amplitude of 50×10^{-6} at the top of the sample. The mass m of the mobile equipment overhead is 0.235 kg (Fig. 1b). The maximum force F_0 and the phase angle Φ were measured during the last ten seconds of the test. The enclosure is piloted and the temperature remains constant during the test.

To identify the viscoelastic properties of the asphalt mixture, first the real part E_1 and the imaginary part E_2 of the complex modulus E^* must be calculated. These values are given by the Eqs. 1 and 2:

$$E_1 = \gamma \left(\frac{F_0}{z_0} \cos(\Phi) + 10^{-6} \mu \omega^2 \right) \tag{1}$$

$$E_2 = \gamma \frac{F_0}{z_0} \sin(\Phi) \tag{2}$$

where ω is the angular frequency, γ (mm^{-1}) is a shape factor depending on the dimensions of the specimen: B = 56 mm, b = 25 mm, e = 25 mm and h = 250 mm (Fig. 1a) and μ is the mass factor, described by:

$$\gamma = \frac{12h^3}{e(B-b)^3} \left[\left(2 - \frac{b}{2B} \right) \frac{b}{B} - \frac{3}{2} - \ln \frac{b}{B} \right] \tag{3}$$

$$\mu = 0.135M + m \tag{4}$$

Finally, the dynamic properties can be determined as:

$$|E^*| = \sqrt{E_1^2 + E_2^2} \tag{5}$$

$$\Phi = \arctan(E_2/E_1) \tag{6}$$

3. Numerical procedures

In this section, the Contact Dynamics (CD) method is briefly introduced, as a discrete approach for the simulation of asphalt mixtures, as well as the numerical procedures used for the preparation of the numerical samples, the proposed viscoelastic contact model and its calibration.

3.1. Numerical method

The 2PB tests simulations were conducted using the LMGC90 software (*LMGC90*, 2021), which is dedicated to multiple physics simulation of discrete material and structures (Dubois & Jean, 2003). This software is based on the Contact Dynamics (CD) method (Brogliato, 1999; Jean, 1999; J. Moreau, 1994; J. J. Moreau, 1988; Radjai & Richefeu, 2009).

The CD method is a particle-based approach for the modeling of non-smooth mechanics in granular systems. The main difference between this approach and the distinct element method (Cundall, 1971, 1988; Cundall & Strack, 1979) or molecular dynamics (Brilliantov, Spahn, Hertzsch, & Pöschel, 1996; Herrmann & Luding, 1998; Pöschel & Buchholtz, 1995; Radjaï & Dubois, 2011) lies in the formulation of the

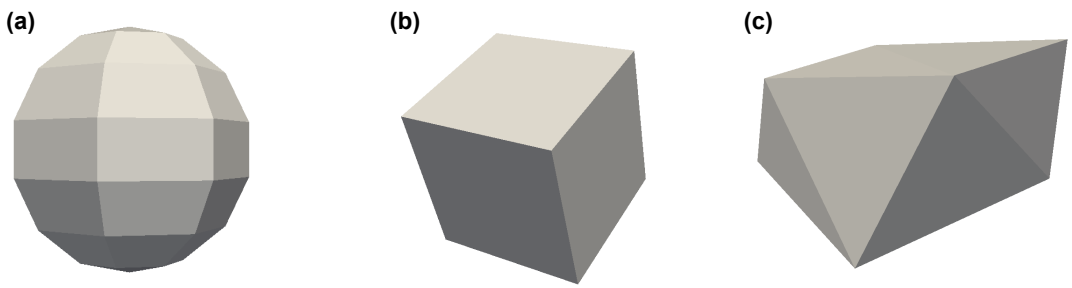

Figure 2. Examples of created particles with different shapes : (a) sphere; (b) regular polyhedron; (c) irregular polyhedron.

contact models as complementary relations between impulses and velocities at the particle-scale. Here, the unilateral contact interactions and Coulomb friction law guarantee the non-interpenetration between perfectly-rigid particles.

The contact detection between two particles is carried out at two levels. First a so-called coarse detection is carried out using the "bounding box" algorithm in order to identify the particles in the neighboring of a reference particle. When two particles are close enough, a finer detection is performed using the "common-plane" method (Cundall, 1988).

3.2. Sample preparation

In the aim to perform the modeling campaign for the 2PB tests, four specimens for three different particle shapes: spherical, regular and irregular polyhedra were prepared numerically, considering the same dimensions displayed in Fig. 1a and the total mass (0.6 kg) of samples used in experimental trials. This numerical campaign was conducted for six temperatures and five frequencies.

To prepare the numerical samples, initially, about 10,000 spherical rigid particles are created following the PSD of a BBSG 0/10 (Tab. 1) cut at 2 mm, in order to reduce the total quantity of elements in the sample, where the fines are included in the mortar phase. This numerical trick reduces the computational time in the simulations. This approach can have an influence on the mechanical response of numerical samples. Future work will be devoted to analyze the effect of the cut size on the mechanical behavior of numerical tests. The initial bulk density of these particles is 2647 kg.m^{-3}. These particles are poured into a box composed of six plates with dimensions: 0.25 m length, 0.025 m width and 1.6 m height. Here, the coefficient of friction among all elements is reduced to 0.1 to generate a dense initial sample.

From each original spherical sample, samples composed of regular and irregular polyhedra were created (Fig. 2). For the case of regular polyhedra, each sphere is replaced by a regular polyhedron composed of eight vertices and six faces (cubes), where the original spheres circumscribe each polyhedron. On the other hand, in the aim to reproduce realistic aggregates, irregular polyhedra were created, where the shape and dimensions of each particle are based on the PSD, the flakiness index of experimental aggregates and statistic data from actual aggregates. Each irregular polyhedron is circumscribed by an ellipsoid surface defined by the following parametric equations (Eq. 7):

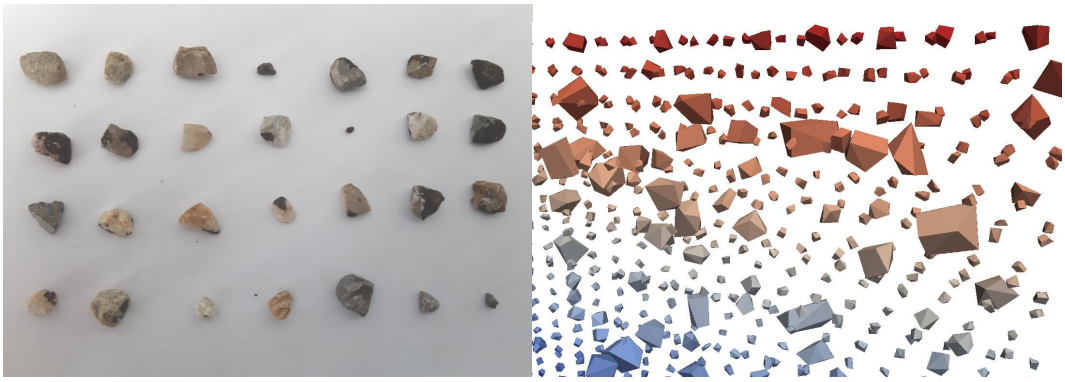

(a) (b)

Figure 3. (a) Actual aggregates used in the visual identification of the shape and the number of vertices. (b) Snapshot of aggregates generated numerically.

$$\begin{cases} x &= S_f \times r\cos(\theta)\cos(\varphi) \\ y &= r\cos(\theta)\sin(\varphi) \\ z &= r\sin(\theta)/S_f \end{cases} \tag{7}$$

where the angles θ and φ vary in the ranges $-\pi/2 \leq \theta \leq \pi/2$ and $-\pi \leq \varphi \leq \pi$, r is the half dimension from the PSD and S_f is a shape factor. The S_f value was varied randomly between 1.0 and 1.5. This factor reproduces the elongation and the flakiness of experimental aggregates on the numerical particles, where the flakiness index (FI) is equals to 17%. This procedure generates different ellipsoid surfaces, where are placed randomly eight vertices. This vertex number was identified visually from 28 experimental aggregates (Fig. 3a) where the average number is equals to 7.77, and the standard deviation is 0.916. This protocol creates convex polyhedrons, based on simplified shapes of actual aggregates, without using complex imaging technics. A snapshot of the numerically generated particles with this protocol is displayed in Fig. 3b.

After the particle replacement stage, the generated numerical slab is cut to obtain the same dimensions as the experimental samples. This procedure is conducted by eliminating the particles where their barycenter is outside the trapezoidal volume showed in Fig. 1a. Then each numerical sample is subjected to a rotation of 90 degrees counter clockwise, changing the gravity direction. Afterwards, each sample is fixed to a bottom and top plates. The latter models the mobile plate of 0.235 kg mass in the experimental set-up.

To take into account the mortar phase surrounding the aggregates, the particle sizes are reduced considering the binder content. For each particle, its radius (or vertex coordinates for polyhedra) is multiplied by a reduction factor r_f calculated as:

$$r_f = \left(1 - T_L \frac{\rho_S}{\rho_L}\right)^{1/3} \tag{8}$$

where T_L is the binder content of 5.6% for experimental samples, ρ_S the initial bulk density of particles equals to 2647 kg.m^{-3}, and ρ_L the binder bulk density of 1030

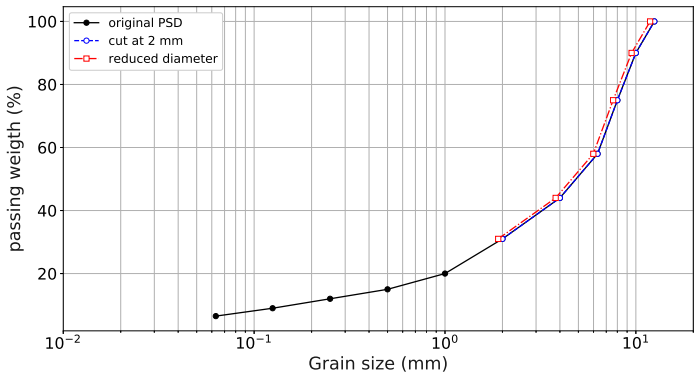

Figure 4. Comparison between the original PSD of aggregates, the cut PSD at 2 mm and the PSD shifted by the reduction factor.

kg.m^{-3}. After this procedure, the bulk density of particles is increased to an average value of 3556 kg.m^{-3}, to reach the experimental total mass of 0.6 kg. The variation in the particle size generates a small shift regarding the original size distribution (Fig. 4). This shift can induce a difference in the mechanical behavior of the sample in comparison with the original PSD. At this stage, the particle-particle friction was set to $\mu = 0.7$ which is a common value employed for crushed aggregates.

Finally, a stabilization step is performed, where the sample is subject only to gravity until reach the equilibrium state. One snapshot of resulting samples composed of different particle shapes is provided in Fig. 5.

3.3. Contact model

At this stage, a viscoelastic contact law was applied between particles, based on the Burgers model (Betten, 2008; Liu & You, 2009), which describes quite well the mechanical performances of asphalt mixtures, such as relaxation, creep and dynamic response (Cai, McDowell, & Airey, 2014; A. C. Collop, McDowell, & Lee, 2006; McDowell et al., 2009; Quezada & Chazallon, 2020). This constitutive model is composed of a Maxwell section and a Kelvin-Voigt section, in series. Four parameters describe its mechanical behavior: the Maxwell's stiffness and viscosity E_m and η_m, and the Kelvin-Voigt's stiffness and viscosity E_k and η_k. Due to the Maxwell dashpot, this model is not suitable for predicting the mechanical response at very low-frequencies, showing some divergences regarding experimental data. This contact law manages the interaction of rigid particles surrounded by a viscoelastic phase (Quezada & Chazallon, 2020).

From this macroscopic description the normal model parameters at the particle-scale can be assessed as follows:

$$K_{m_n} = \frac{\pi r_{min}^2}{l_0} E_m \tag{9}$$

$$C_{m_n} = \frac{\pi r_{min}^2}{l_0} \eta_m \tag{10}$$

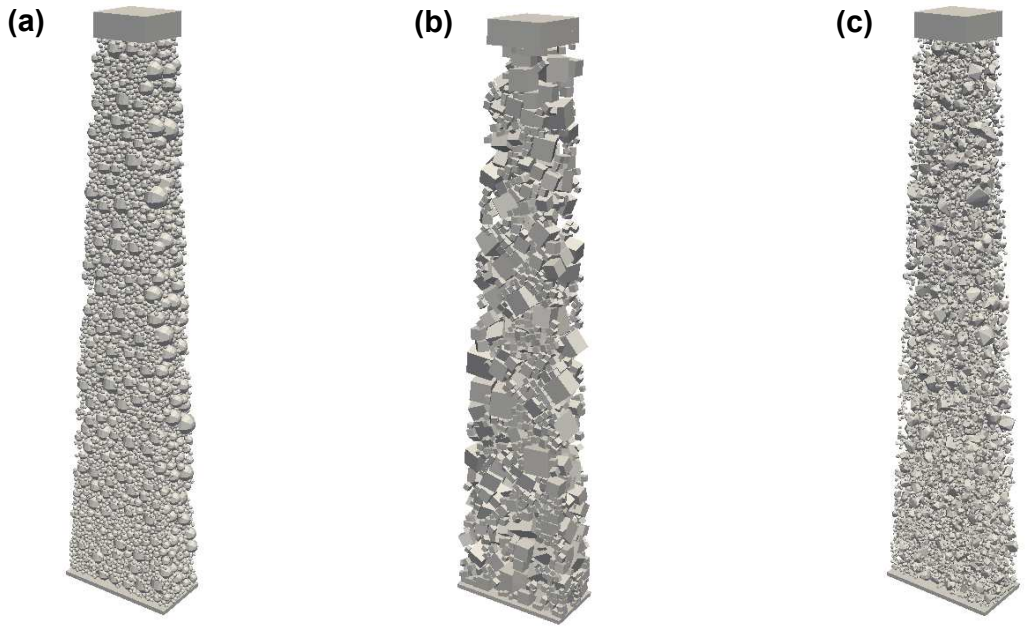

Figure 5. Snapshot of numerical samples after the preparation stage: (a) Spherical sample; (b) Regular polyhedral sample; (c) Irregular polyhedral sample

$$K_{k_n} = \frac{\pi r_{min}^2}{l_0} E_k \tag{11}$$

$$C_{k_n} = \frac{\pi r_{min}^2}{l_0} \eta_k \tag{12}$$

where K_{m_n}, C_{m_n}, K_{k_n} and C_{k_n} are the normal stiffness and viscosities at the particle-scale, r_{min} is the minimum radius of two particles at contact and l_0 is the initial gap between the mass center of these particles (see Fig. 6).

On the other hand, the tangential components of the contact model for both tan-

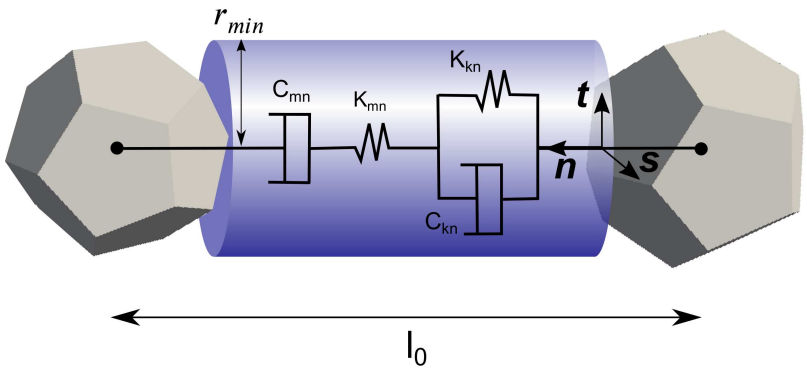

Figure 6. Contact law based on the Burgers model

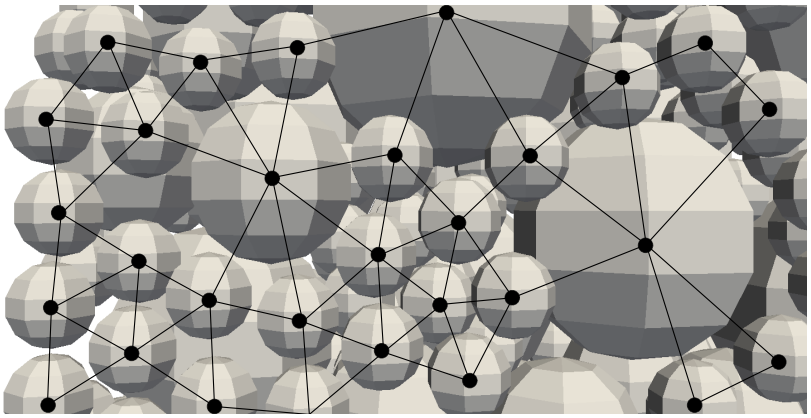

Figure 7. Representation of particles linked by the viscoelastic contact model within a spherical sample.

gential directions can be computed from the above normal parameters, considering an isotropic behavior, as:

$$K_{m_t} = \frac{K_{m_n}}{2(1+\nu)} \tag{13}$$

$$C_{m_t} = \frac{C_{m_n}}{2(1+\nu)} \tag{14}$$

$$K_{k_t} = \frac{K_{k_n}}{2(1+\nu)} \tag{15}$$

$$C_{k_t} = \frac{C_{k_n}}{2(1+\nu)} \tag{16}$$

where ν is the Poisson's ratio. For the sake of simplicity, this ratio was set to 0.35 (Cai et al., 2014; A. C. Collop et al., 2006). The temperature can modify the value of the Poisson's ratio, which can vary between 0.35 and 0.5 for asphalt mixes. Further works will take into account the variation of the Poisson's ratio with the temperature and its effect on the mechanical performances of the model. This procedure creates from only four macroscopic parameters a set of parameters at the particle-scale equals to the total number of contacts within an asphalt mixture.

The proposed contact model links each particle with their neighbors. In order to consider the viscoelastic contact between two particles, the gap between them must be less than 1 mm, where this value corresponds to the minimal half dimension of particles in the sample. This gap value was calibrated for the current particle sample, where this is the minimal value that ensures a stabilization of the number of contact of neighboring particles within the sample. With this procedure, an initial network of viscoelastic contacts is created at the beginning of the simulation. An example of this network is displayed in Fig. 7.

3.4. Complex modulus test modeling

The numerical tests were performed by subjecting the top plate to a sinusoidal displacement with amplitude A=63×10^{-6} m, as experimental trials, during five cycles. The displacement and the total reaction at the top plate are measured throughout the test. Then the peak force F_0 and peak displacement z_0 are identified to determine the numerical values of $|E^*|$ and Φ. The time step was set to 5×10^{-5} s in all simulations to ensure the convergence of the numerical resolution. From this time step length, force values gather in the same curve evolution (Quezada & Chazallon, 2020). The number of time steps needed to perform five loading cycles varies from 3.33×10^4 to 2.5×10^3 for 3 Hz and 40 Hz respectively, where the computational time was comprises between 1.7 and 22 hours. The CPU time was 2×10^{-4} s per particle and per time step on a Dell computer of speed 2.1 GHz.

3.4.1. Calibration of the numerical modeling

In the aim to calibrate the contact model parameters regarding the experimental data, an analytical macroscopic approach was adopted, based on the constitutive Burgers model. For the complex modulus test, the viscoelastic material properties can be determined from the complex compliance:

$$|D^*| = \sqrt{D'(\omega)^2 + D''(\omega)^2} \tag{17}$$

where D' and D'' correspond to the real and imaginary parts, respectively. Both real and imaginary parts of the complex compliance can be calculated using the macroscopic Burgers model parameters as:

$$D'(\omega) = \frac{1}{E_m} + \frac{E_k}{E_k^2 + \omega^2 \eta_k^2} \tag{18}$$

$$D''(\omega) = \frac{1}{\omega \eta_m} + \frac{\omega \eta_k}{E_k^2 + \omega^2 \eta_k^2} \tag{19}$$

Based on these analytical expressions, it is possible to determinate the Burgers model parameters to reproduce the evolution of $|E^*|$ and Φ. The norm of the complex modulus can be obtained by $|E^*| = |D^*|^{-1}$ and the associated phase angle as $\Phi = \arctan(D''/D')$.

For the calibration of the Burgers model parameters, an iterative procedure was set up for each temperature (Fig. 8), where each step is described as follows:

(1) First, a numerical simulation is performed using a set of initial Burgers parameters for each loading frequency.

(2) Then, the numerical values for $|E^*|$ and Φ are computed using the Eqs. 1 to 6.

(3) The numerical values obtained from this simulation are compared with those assessed from the analytical model (Eqs. 17 to 19) with the same set of parameters. During the iteration process a difference for the predicted values between

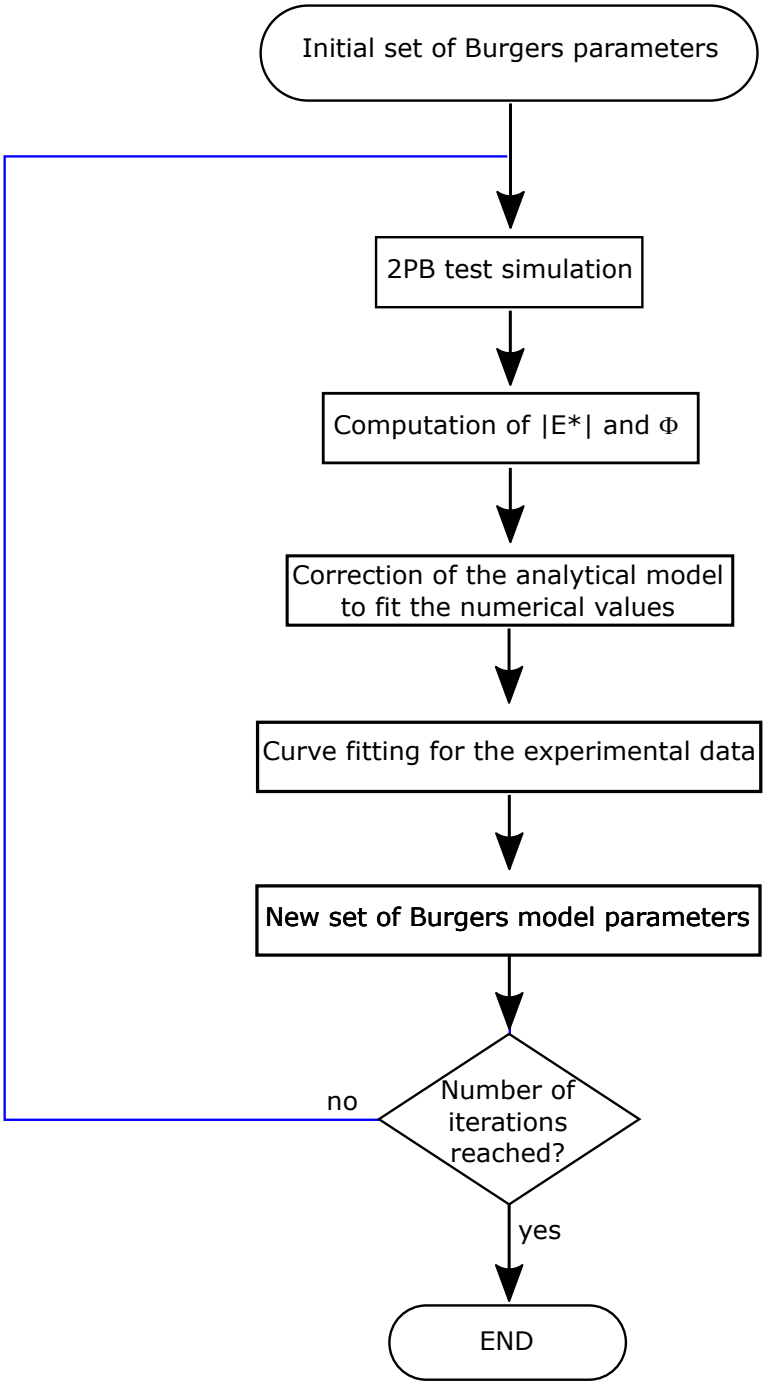

Figure 8. Flowchart for the calibration of Burgers parameters.

Table 2. Average values for the correction factors between analytical and numerical model.

	Correction factor	
Shape	α	β
Polyhedron	56.83	48.10
Sphere	50.64	61.18
Cube	27.51	28.55

the analytical model and the numerical modeling was observed. In order to compensate this difference, a correction on the analytical expressions of the real and imaginary part of the complex modulus is proposed as follows:

$$E_1^c = E_{an} \cos(\Phi_{an})\alpha \tag{20}$$

$$E_2^c = E_{an} \sin(\Phi_{an})\beta \tag{21}$$

where E_1^c and E_2^c are the corrected values for the real and imaginary part of the complex modulus, E_{an} and Φ_{an} correspond to the values obtained from the fitting with the analytical model, and α and β are dimensionless correction factors. These correction factor were calculated using a curve fitting by means an optimization algorithm from Python programming language (*Python Software Foundation*, 2021), performing a non-linear least squares method. The obtained average values for the correction factors are displayed in Table 2 as a function of the particle-shape. The correction factors from the analytical to the numerical model seem to be a function of the size distribution and morphology of the aggregates. Future works will focus specifically in the features linked to aggregates morphology.

(4) The corrected analytical expressions are employed afterwards to fit the experimental $|E^*|$ and Φ values. Here, the curve fitting procedure provides the best-fit parameters for each temperature. Using the corrected expressions from Eqs. 20 and 21 allows to estimate the values of the numerical model directly from the experimental tests.

(5) Finally, the new set of parameters is used to perform a new calculation for the next iteration step.

Table 3 displays the calibrated parameters obtained with the described procedure. Five iteration steps were needed for each temperature and each sample to determinate these Burgers model parameters. The parameter calibration of the Burgers model makes it possible to represent also different types of mortar.

Table 3. Macroscopic Burgers model parameters used in the numerical simulations.

	Burgers parameters			
T (^{o}C)	E_m (Pa)	η_m (Pa.s)	E_k (Pa)	η_k (Pa.s)
-10	4.56×10^8	6.33×10^8	9.67×10^9	1.27×10^8
0	4.23×10^8	2.09×10^8	2.68×10^9	2.42×10^7
10	3.41×10^8	6.55×10^7	9.52×10^8	1.09×10^7
15	3.09×10^8	3.42×10^7	5.69×10^8	6.75×10^6
20	2.74×10^8	1.57×10^7	3.25×10^8	3.88×10^6
30	1.88×10^8	2.99×10^6	1.11×10^8	1.26×10^6

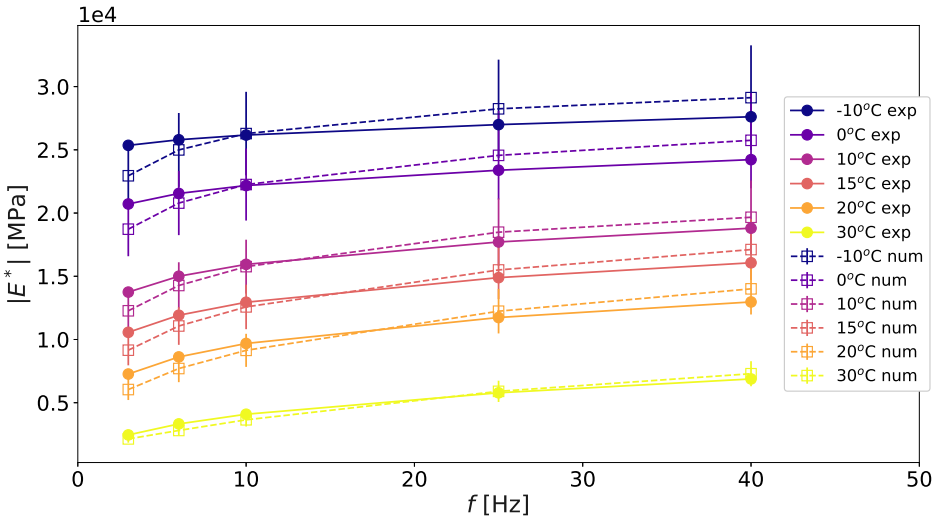

Figure 9. Norm of complex modulus $|E^*|$ isotherms for experimental and numerical polyhedral samples. Here, the error bar is plotted using one standard deviation.

4. Validation of the numerical modeling

In the aim to validate the proposed numerical approach, Fig. 9 and 10 displays the comparison between the experimental and numerical results for the norm of complex modulus and phase angle isotherms for polyhedral samples. Numerical data of $|E^*|$ and Φ follow the experimental values, despite some fluctuations around the average values. One can observe a larger variation in numerical $|E^*|$ values for low-temperatures. For Φ values, the fluctuations are larger for a frequency of 40 Hz, while a separation for high-temperatures and low frequencies can be noticed.

To identify the effect of the particle shape on the sample viscoelastic performances, the master curves were computed for both $|E^*|$ and Φ values for all samples. To build each master curve, a reference temperature T_{ref} =15 ^{o}C was chosen. Then, the translation of all isotherm curves is performed by calculating the reduced frequency as: $a_T f = f \times 10^{a_T}$, where f corresponds to each frequency value in each curve and a_T is the shift factor. Figure 11 displays the shift factor values as a function of the temperature. These values are obtained from the fit with the temperatures ones using the Williams-Landel-Ferry (WLF) equation:

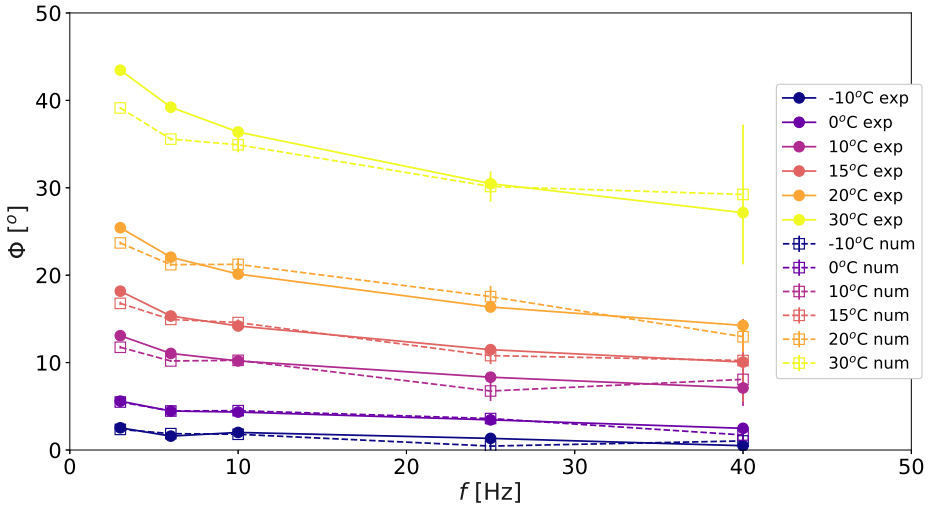

Figure 10. Phase angle Φ isotherms for experimental and numerical polyhedral samples. Here, the error bar is plotted using one standard deviation.

Table 4. Shift factor values for each temperature.

T (^{o}C)	-10	0	10	15	20	30
$\log(a_T)$	3.8	2.3	0.65	0.0	-0.7	-1.85

$$\log(a_T) = \frac{-C_1(T - T_{ref})}{C_2 + (T - T_{ref})} \tag{22}$$

where C_1 and C_2 are 28 and 206.8 ^{o}C respectively, and T is the temperature. Figures 12 and 13 display the resulting curves for experimental and numerical results as a function of the particle shape. It should be noted that the parameters of the Burgers model (Table 3) can be determined from the master curves for the reference temperature of 15 ^{o}C. We can define a constant value for the Maxwell stiffness at 15 ^{o}C, which has a purely elastic behavior, while for the other parameters, we can translate them using the shift factor a_T together with the reference temperature parameters. In other words, the calibration process ensures indirectly the time-temperature superposition principle (TTSP).

Regarding the $|E^*|$ master curve, polyhedral samples show a good prediction of $|E^*|$ values, while for the samples composed of spheres, the values of the norm of the complex modulus are slightly underestimated. On the contrary, for cubical samples the $|E^*|$ curve is completely shifted. Building a sample with cubic particles results in a looser sample and with a lower number of contacting particles compared to samples made up of spheres or irregular polyhedrons. This results in the generation of a weaker contact network and consequently in a weaker mechanical response, regarding $|E^*|$. For the case of Φ master curve values, the most part of the data collapse in the same curve, regardless the particle shape. From these observations, it can be concluded that the particle shape does not have a significant influence on the values of the phase angle. On the other hand, the values of the norm of the complex modulus are more sensitive

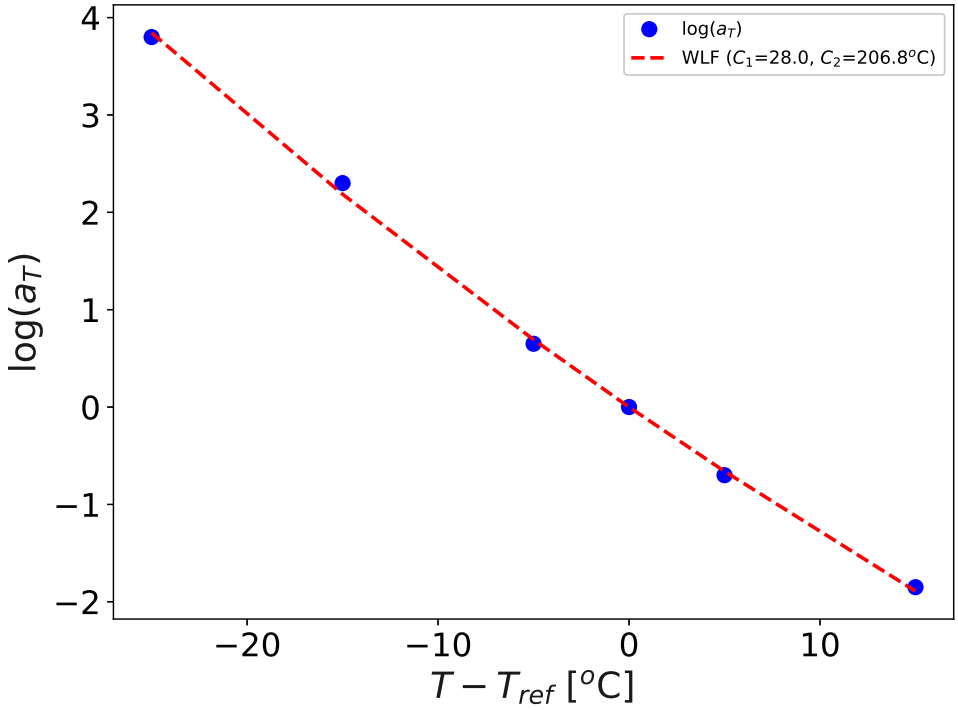

Figure 11. Shift factor values as a function of temperature.

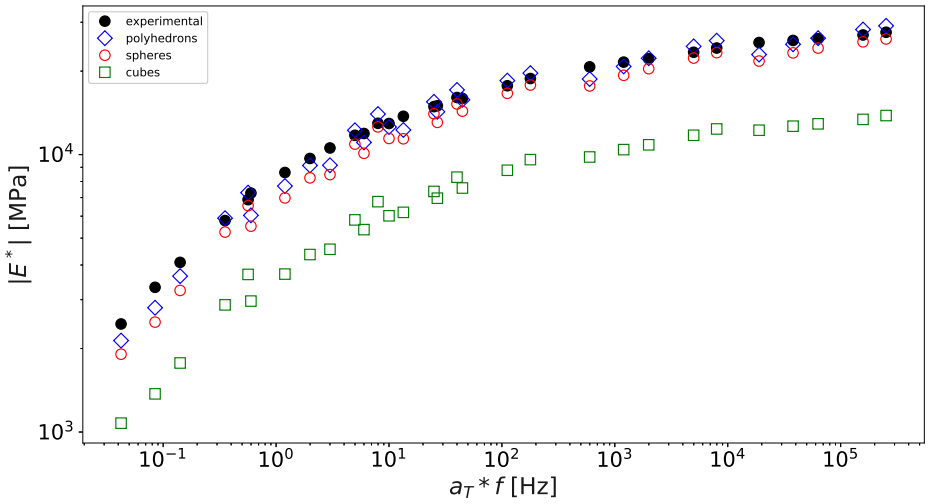

Figure 12. Complex modulus master curve for experimental tests and numerical simulations. (T_{ref} =15^{o}C).

to the change of the shape of the particles. This is due to the contact surface between the particles and to the contact and force network generated inside each sample. A more realistic particle shape achieves a more accurate estimation of the mechanical performance of bituminous mixes.

To analyze the asymptotic behaviors of the studied asphalt material (low-temperature/high-frequency or high-temperature/low-frequency), the Cole-Cole plan and the Black diagram were plotted for polyhedral samples. Figure 14 displays the Cole-Cole plane analysis where E_2 values are plotted against E_1 values. This graph emphasizes the behavior of asphalt mixtures at low-temperature/high-frequency conditions. In this curve numerical results show some fluctuations around the experimental values in the curve. These variations are induced in part by the prediction of the phase angle values Φ in isotherm curves (Fig. 13), where for the case of high-temperatures the estimation of numerical data show some deviations regarding experimental values. Despite these fluctuations, numerical results follow the average trend in experimental data, showing a more accurate prediction towards the asymptotic values.

To study the behavior at high-temperature/low-frequency for the bituminous material in this work, Fig. 15 shows the Black diagram. This graph was built by plotting $|E^*|$ values as a function of Φ values. In this figure is possible to observe the asymptotic behavior with the phase angle Φ equal to zero ($|E^*|$ about $2.8{\times}10^4$ MPa. The experimental and numerical data are in good agreement for Φ values less than 30^o. From this threshold, the numerical values fall.

In both figures, all data collapse in the same average trend and temperature influence is not visible. Therefore, these results confirm the frequency-temperature superposition principle regarding the equivalence of the effects of frequency and temperature on the material behavior. The fluctuations observed between experimental and numerical data may be induced by some limitations of the Burgers contact model.

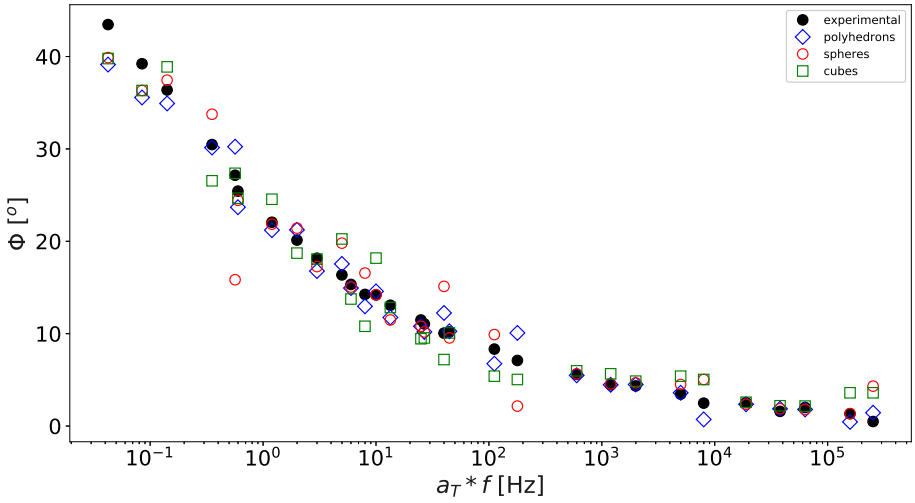

Figure 13. Phase angle master curve for experimental tests and numerical simulations. (T_{ref} =15^{o}C).

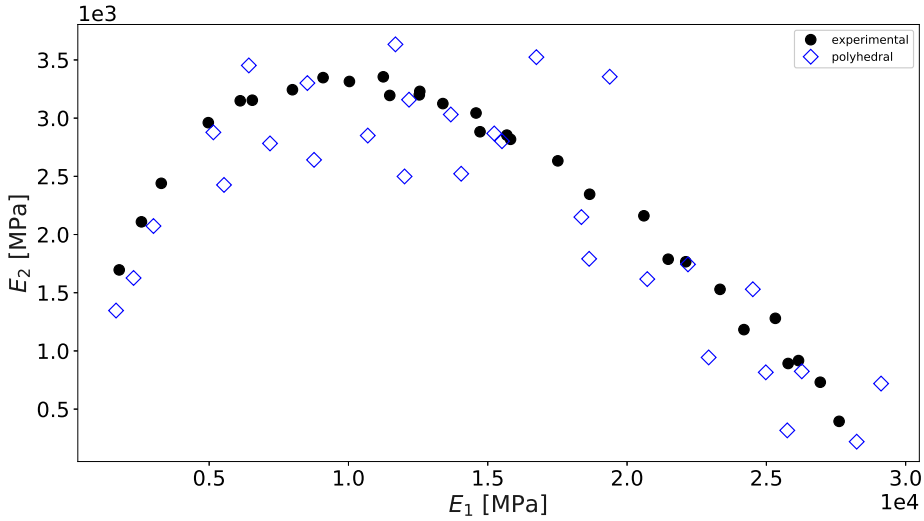

Figure 14. Cole-Cole plot for experimental tests and numerical simulations.

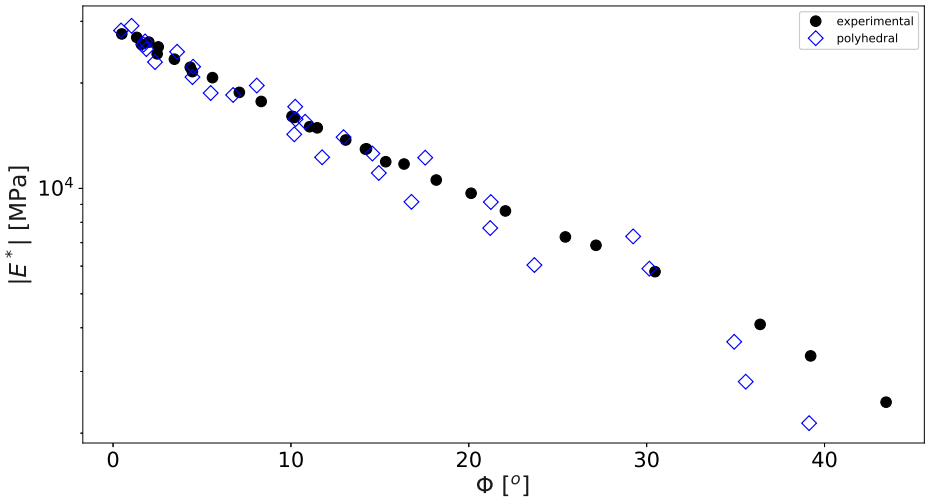

Figure 15. Black diagram for experimental and numerical results.

5. Concluding remarks

In this paper discrete simulations of complex modulus tests in a 2PB configuration were presented. The numerical specimens were prepared using spherical, regular and irregular polyhedral particles. For the latter, the particle-generation procedure was based on statistic criteria to reproduce the elongation, flakiness and the number of vertices identified from actual aggregates, without using 3D scan or other imaging technics. The mortar phase was modeled using a contact law between particles based on the constitutive Burgers model. The numerical campaign reproduces the experimental tests, where four trapezoidal samples were subjected to five frequencies and six temperatures.

The main outcomes in this study are enumerated below:

- The numerical simulations with irregular polyhedral are able to reproduce the complex modulus properties of bituminous materials. For different analysis conducted in this paper, the numerical results of these simulations were in a good agreement regarding experimental data.

- The iterative procedure used for the calibration of model parameters adapts the analytical expressions for numerical samples, by using correction factors. These corrected expressions allow the parameters of the Burgers contact model to be obtained directly from the isotherm curves.

- For isotherm curves, numerical data of the norm of the complex modulus $|E^*|$ and the phase angle Φ values follow the trend of experimental values, despite some fluctuations around the average values. Certain lack of accuracy in the prediction of the experimental values may be due to the limitations of the contact model. Future research will focus on the use of other contact models, such as the generalized Maxwell model or the VENoL model (Coulon, Koval, Chazallon, & Roux, 2021).

- With respect to the master curves, for the case of Φ, all the numerical values show a good agreement with the experimental values, regardless of the shape of the particles that make up each sample. However, the influence of the particle shape is more visible in the calculation of the $|E^*|$ values, where a less realistic shape leads to underestimate these numerical values. This difference could come from the determination of the contact areas between particles and the arrangement of the particles in the sample, where granular fabric is different. Future works will focus specifically in the features linked to aggregates morphology.

- Regarding the Cole-Cole plan and Black diagram, the equivalence of the effects of frequency and temperature on material behavior was verified. Here, the numerical data ensures indirectly the time-temperature superposition principle (TTSP). Both numerical and experimental data can be represented as a single curve, where asymptotic behavior can be identified where Φ values reach zero.

In conclusion, this preliminary work can be considered as encouraging for the validation of the proposed numerical approach for the study of asphalt mixtures features such as creep, rutting and fatigue cracking performance.

Funding

The work presented in this paper was sponsored by the French National Research Agency (ANR - SolDuGri project ANR-14-CE22-0019).

Acknowledgments

The authors want to thank Colas S.A. for providing the experimental data.

References

Abbas, A., Masad, E., Papagiannakis, T., & Harman, T. (2007). Micromechanical modeling of the viscoelastic behavior of asphalt mixtures using the discrete-element method. *International journal of geomechanics*, *7*(2), 131–139.

Alonso-Marroquin, F., & Herrmann, H. (2002). Calculation of the incremental stress-strain relation of a polygonal packing. *Physical Review E*, *66*(2), 021301.

Ameri, M., Mansourian, A., Khavas, M. H., Aliha, M., & Ayatollahi, M. (2011). Cracked asphalt pavement under traffic loading–a 3d finite element analysis. *Engineering Fracture Mechanics*, *78*(8), 1817–1826.

Azéma, E., Radjai, F., & Dubois, F. (2013). Packings of irregular polyhedral particles: Strength, structure, and effects of angularity. *Physical Review E*, *87*(6), 062203.

Azéma, E., Radjai, F., & Saussine, G. (2009, June). Quasistatic rheology, force transmission and fabric properties of a packing of irregular polyhedral particles. *Mechanics of Materials*, *41*(6), 729–741.

Bai, T., Cheng, Z., Hu, X., Fuentes, L., & Walubita, L. F. (2020). Viscoelastic modelling of an asphalt pavement based on actual tire-pavement contact pressure. *Road Materials and Pavement Design*, 1–20.

Betten, J. (2008). *Creep mechanics*. Springer Science & Business Media.

Brilliantov, N. V., Spahn, F., Hertzsch, J.-M., & Pöschel, T. (1996). Model for collisions in granular gases. *Physical review E*, *53*(5), 5382.

Brogliato, B. (1999). *Nonsmooth mechanics*. London: Springer.

Buttlar, W. G., & You, Z. (2001). Discrete element modeling of asphalt concrete: microfabric approach. *Transportation Research Record*, *1757*(1), 111–118.

Cai, W., McDowell, G., & Airey, G. (2014). Discrete element visco-elastic modelling of a realistic graded asphalt mixture. *Soils and Foundations*, *54*(1), 12–22.

Cantor, D., Azéma, E., Sornay, P., & Radjai, F. (2017). Numerical simulation of the compaction of crushable grains in 3d. In *Epj web of conferences* (Vol. 140, p. 07016).

Chabot, A., Chupin, O., Deloffre, L., & Duhamel, D. (2010). Viscoroute 2.0 a: tool for the simulation of moving load effects on asphalt pavement. *Road Materials and Pavement Design*, *11*(2), 227–250.

Chazallon, C., Koval, G., Hornych, P., Allou, F., & Mouhoubi, S. (2009). Modelling of rutting of two flexible pavements with the shakedown theory and the finite element method. *Computers and Geotechnics*, *36*(5), 798–809.

Collop, A., Scarpas, A., Kasbergen, C., & de Bondt, A. (2003). Development and finite element implementation of stress-dependent elastoviscoplastic constitutive model with damage for asphalt. *Transportation Research Record: Journal of the Transportation Research Board*(1832), 96–104.

Collop, A. C., McDowell, G. R., & Lee, Y. W. (2006). Modelling dilation in an idealised asphalt mixture using discrete element modelling. *Granular Matter*, *8*(3-4), 175–184.

Coulon, L., Koval, G., Chazallon, C., & Roux, J.-N. (2021). Analytical modelling of thixotropy contribution during t/c fatigue tests of asphalt concrete with the venol model. *Road Materials and Pavement Design*, *22*(sup1), S536–S559.

Cundall, P. A. (1971). A computer model for simulating progressive, large scale movement in blocky rock systems. In *Symp. isrm, nancy, france, proc.* (Vol. 2, pp. 129–136).

Cundall, P. A. (1988). Formulation of a three-dimensional distinct element model—part i. a scheme to detect and represent contacts in a system composed of many polyhedral blocks. In *International journal of rock mechanics and mining sciences & geomechanics abstracts* (Vol. 25, pp. 107–116).

Cundall, P. A., & Strack, O. D. (1979). A discrete numerical model for granular assemblies. *Geotechnique*, *29*(1), 47–65.

Dai, Q., & You, Z. (2007). Prediction of creep stiffness of asphalt mixture with micromechanical finite-element and discrete-element models. *Journal of Engineering Mechanics*, *133*(2), 163–173.

Dondi, G., Vignali, V., Pettinari, M., Mazzotta, F., Simone, A., & Sangiorgi, C. (2014). Modeling the dsr complex shear modulus of asphalt binder using 3d discrete element approach. *Construction and building Materials*, *54*, 236–246.

Dubois, F., & Jean, M. (2003). Lmgc90. In *Actes du sixieme colloque national en calcul des structures* (Vol. 1, pp. 111–118).

En 12697-26: Bituminous mixtures. test methods for hot mix asphalt. part 26: Stiffness. (AFNOR ed.) [Computer software manual]. (2012).

Fedele, R., Praticò, F. G., & Pellicano, G. (2019). The prediction of road cracks through acoustic signature: Extended finite element modeling and experiments. *Journal of Testing and Evaluation*, *49*(4), 2942–2963.

Gao, X., Koval, G., & Chazallon, C. (2019). A discrete element model for damage and fatigue crack growth of quasi-brittle materials. *Advances in Materials Science and Engineering*, *2019*.

He, X., Abdelaziz, S., Chen, F., & Yin, H. (2019). Finite element simulation of self-heated pavement under different mechanical and thermal loading conditions. *Road Materials and Pavement Design*, *20*(8), 1807–1826.

Herrmann, H., & Luding, S. (1998). Modeling granular media on the computer. *Continuum Mechanics and Thermodynamics*, *10*(4), 189–231.

Jean, M. (1999). The non smooth contact dynamics method. *Computer Methods in Applied*

Mechanic and Engineering, *177*, 235-257.
Kim, Y.-R., Allen, D., & Little, D. (2007). Computational constitutive model for predicting nonlinear viscoelastic damage and fracture failure of asphalt concrete mixtures. *International Journal of Geomechanics*, *7*(2), 102–110.
Kim, Y.-R., & Aragão, F. T. S. (2013). Microstructure modeling of rate-dependent fracture behavior in bituminous paving mixtures. *Finite Elements in Analysis and Design*, *63*, 23–32.
Li, M., Wang, H., Xu, G., & Xie, P. (2017). Finite element modeling and parametric analysis of viscoelastic and nonlinear pavement responses under dynamic fwd loading. *Construction and Building Materials*, *141*, 23–35.
Liu, Y., & You, Z. (2009). Determining burger's model parameters of asphalt materials using creep-recovery testing data. In *Pavements and materials: Modeling, testing, and performance* (pp. 26–36).
Lmgc90. (2021). `https://git-xen.lmgc.univ-montp2.fr/lmgc90/lmgc90_user/-/wikis/home`.
Lu, M., & McDowell, G. (2007). The importance of modelling ballast particle shape in the discrete element method. *Granular matter*, *9*(1-2), 69–80.
Lu, Y., & Wright, P. (1998). Numerical approach of visco-elastoplastic analysis for asphalt mixtures. *Computers & structures*, *69*(2), 139–147.
Masad, E., & Somadevan, N. (2002). Microstructural finite-element analysis of influence of localized strain distribution on asphalt mix properties. *Journal of engineering mechanics*, *128*(10), 1105–1114.
McDowell, G., Collop, A., & Wu, J. (2009). A dimensional analysis of scaling viscosity and velocity in dem of constant strain rate tests on asphalt. *Geomechanics and Geoengineering: An International Journal*, *4*(2), 171–174.
Moreau, J. (1994). Some numerical methods in multibody dynamics: Application to granular materials. *European Journal of Mechanics A/Solids*, *supp.*(4), 93-114.
Moreau, J. J. (1988). Unilateral contact and dry friction in finite freedom dynamics. In *Cism* (p. 1-82).
Nguyen, M., Froiio, F., Cambou, B., Di Benedetto, H., & Sauzéat, C. (2016). Simulation of the asymptotic behaviour of bituminous mixtures using the discrete element method. In *8th rilem international conference on mechanisms of cracking and debonding in pavements* (pp. 39–45).
Pöschel, T., & Buchholtz, V. (1995). Molecular dynamics of arbitrarily shaped granular particles. *J. Phys. I France*, *5*(11), 1431-1455.
Python software foundation. (2021). `https://www.python.org/`.
Quezada, J. C., Breul, P., Saussine, G., & Radjai, F. (2012). Stability, deformation, and variability of granular fills composed of polyhedral particles. *Physical Review E*, *86*(3), 031308.
Quezada, J. C., & Chazallon, C. (2020). Complex modulus modeling of asphalt concrete mixes using the non-smooth contact dynamics method. *Computers and Geotechnics*, *117*, 103255.
Quezada, J. C., Sagnol, L., & Chazallon, C. (2017). Shear test on viscoelastic granular material using contact dynamics simulations. In *Epj web of conferences* (Vol. 140, p. 08009).
Radjaï, F., & Dubois, F. (2011). *Discrete-element modeling of granular materials.* Wiley-Iste.
Radjai, F., & Richefeu, V. (2009). Contact dynamics as a nonsmooth discrete element method. *Mechanics of Materials*, *41*(6), 715–728.
Saint-Cyr, B., Szarf, K., Voivret, C., Azéma, E., Richefeu, V., Delenne, J.-Y., ... others (2012). Particle shape dependence in 2d granular media. *EPL (Europhysics Letters)*, *98*(4), 44008.
Souza, L. T., Kim, Y.-R., Souza, F. V., & Castro, L. S. (2012). Experimental testing and finite-element modeling to evaluate the effects of aggregate angularity on bituminous mixture performance. *Journal of Materials in Civil Engineering*, *24*(3), 249–258.
Yu, H., & Shen, S. (2013). A micromechanical based three-dimensional dem approach to characterize the complex modulus of asphalt mixtures. *Construction and building Materials*,

38, 1089–1096.
Zhou, C., Zhang, M., Li, Y., Lu, J., & Chen, J. (2019). Influence of particle shape on aggregate mixture's performance: Dem results. *Road Materials and Pavement Design*, *20*(2), 399–413.